PCCP

Accepted Manuscript

ROYAL SOCIETY OF CHEMISTRY

www.rsc.org/pccp

Journal Name

RSCPublishing

ARTICLE

Thermal Conductivity of Organic Bulk Heterojunction Solar Cell: *Unusual Binary Mixing Effect*

Cite this: DOI: 10.1039/x0xx00000x

Received 00th January 2012,
Accepted 00th January 2012

DOI: 10.1039/x0xx00000x

www.rsc.org/

Zhi Guo[a], Doyun Lee[b] Joseph Strzalka[c], Haifeng Gao[b], Libai Huang[d], Ali M. Khounsary[e] and Tengfei Luo[a,f],

[6,6]-phenyl-C61-butyric acid methyl ester (PCBM), a fullerene derivative, is the most widely used electron acceptor in bulk-heterojunction (BHJ) organic photovoltaics, and its concentration is usually tuned to achieve optimal device performance. However, PCBM loading can significantly impair the thermal transport performance of the BHJs due to its ultra-low thermal conductivity (0.03-0.07 $Wm^{-1}K^{-1}$). In this work, we study the thermal conductivity of BHJs as a function of PCBM concentration using time domain thermoreflectance. The thermal conductivities of BHJs composed of PCBM blended with donor polymers from the PBDTTT family with different side chains systematically deviate from those predicted by effective medium theory. Evidence presented in this work indicates that for these copolymers, only when polymer concentration reaches a threshold value (~30-35% volumetric fraction), the thermal conductivity BHJ film starts to increase, possibly due to the formation of high thermal conductivity percolation pathways.

Introduction

As an alternative to silicon solar cells, organic polymer solar cells (PSC) are promising photovoltaic solutions because of their low costs, facile fabrication procedure and sufficiently high power conversion efficiency[1-3]. The bulk heterojunction (BHJ) structure, which consists of polymer donor and PCBM acceptor, has been the core of PSC research. Recently, it has been shown that the power conversion efficiency of polymer solar cell based on low-bandgap polymers, poly(4,8-bis-alkyloxybenzo[1,2-b:4,5-b′]dithiophene-2,6-diyl-alt-(alkylthieno[3,4-b]thiophene-2-carboxylate)-2,6-diyl) (PBDTTT), exceeds 10%[1]. Despite the significant progresses in this regard, the thermal transport property in this class of solar cell is largely unknown. Considering the low efficiency of PSCs, the majority of the solar energy received is actually converted into heat. Heat generated through futile charge recombination processes can cause temperature to rise in the solar cell, leading to thermal aging. Thermal aging in BHJ devices results in undesired further phase segregation[4, 5]. The latter has been shown to impair the long-term stability of these device [6, 7] and can even occur at relatively low temperatures (40-50 °C)[8]. Therefore, it is vital to understand the thermal transport properties of the BHJ devices.

Polymers are well-known to have low thermal conductivities (~O(0.1) $Wm^{-1}K^{-1}$) in amorphous states[9, 10]. There are methods to improve polymer thermal conductivity, especially by changing the global morphology, such as forming crystalline polymer fibers[11-17]. It has also been shown that in an amorphous polymer, local morphology related to crystallinity and local characteristic lengths can be tuned to facilitate thermal transport[17, 18]. While amorphous polymers have generally low thermal conductivity, PCBM is reported to have even smaller thermal conductivity (0.03-0.07 $Wm^{-1}K^{-1}$) -- below that predicted by the minimal thermal conductivity model for disordered materials[19, 20]. Although more promising donor polymers are being explored, PCBM has continued to be one of the most efficient and widely used acceptors. Fine tuning the PCBM concentration is a common method to optimize the device power conversion efficiency[21, 22]. However, increasing the PCBM content will inevitably deteriorate the thermal transport performance of BHJs. Hence, it is imperative to understand the impact of the polymer-PCBM mixing ratio on the thermal conductivity of BHJs, which will be useful in achieving a balanced thermal and charge transport performance in PSCs.

BHJs are essentially two-phase composites. Polymer composites with high thermal conductivity inorganic particles have been extensively studied to improve polymer thermal conductivity[23-25]. With almost no exception, the composite thermal conductivity increases as the particle concentration increases[26-29]. However, unlike the filler particles (e.g., metal

powders) that are usually used to improve the low thermal conductivity of polymers, in organic BHJs, the other constituent, PCBM, has an even lower thermal conductivity than those of polymers. The major difference between a polymer-PCBM composite and a polymer-inorganic particle composite is that both constituents in the polymer-PCBM composite can break down to the molecule level when mixing, while the entities of the inorganic particles usually stay intact. Then, will there be a different mixing behavior for the polymer-PCBM composite? Duda et al.[30] studied the thermal conductivity of P3HT:PCBM blend, and found it to have a linear relation with the P3HT concentration. Our previous study on PBDTTT:PCBM BHJs shows very different charge transport behavior from the P3HT:PCBM counterparts due to special morphologies and phase segregation characteristics[31]. It is shown in current work that such structural differences can also lead to distinct thermal transport behavior for the PBDTTT:PCBM blends.

In the present study, we use time domain thermoreflectance (TDTR) measurements to study the thermal conductivity of BHJs made of PCBM and a family of conjugated copolymers (PBDTTT) with different side chain decorations that influences the local morphology of the polymer phase. We have found that the relation between thermal conductivity and composition ratio is not only nonlinear but also deviates from the conventional mixing rules described by effective medium approximation (EMA)[32]. The thermal conductivity change follows a percolation rule with the increase of polymer content in the BHJs, which is further supported by structure as well as morphology characterizations.

Materials and methods

The PBDTTT family of polymers is a class of π-conjugated copolymers. In our study, its backbone is decorated with three substituted alkyl groups (structures shown in Figure 1), which can in turn tune the crystallinity of the polymer. Long and linear side chains confer the polymers with better crystallinity, while short and branched side chains induce more amorphous polymer aggregates[33, 34]. Different side chain combinations result in four different polymers: EE, ED, DE and DD, with increasing crystallinity. Detailed polymer synthesis, film deposition, and neat polymer film thermal conductivity characterization were reported in our previous work[18]. In this work, BHJ films were prepared for the thermal conductivity measurements by spin casting. The PCBM ([6,6]-Phenyl-C61 butyric acid methyl ester, purity >99%) was purchased from American Dye Source Inc. and used without further purification. Polymers were blended with PCBM in a series of volumetric ratios (1:3, 1:2, 1:1, 2:1, and 3:1). The blends were then dissolved in chlorobenzene to achieve polymer concentrations of 20 mg/mL. The solutions were spin cast into films at 1500 rpm for 30 sec. The resulting film thickness determined by profilometry (KLA-Tencor P6) ranges from 55 nm to 72 nm. We here note that copolymers used in this study already provide well-defined phase separation in BHJs and further thermal annealing usually undermines device performance[35-37], which is different from homopolymers like P3HT that require thermal annealing to achieve optimal device performance. As a result, those spin-cast films were characterized and used for TDTR measurements without any thermal annealing.

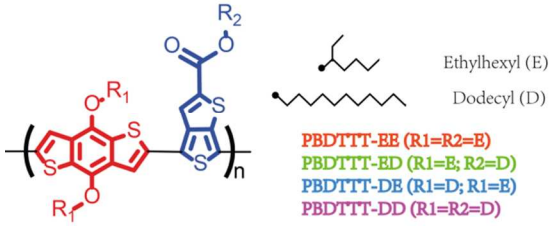

Figure 1. Molecular structure of PBDTTT polymers. The red part is the BDT unit connected with two symmetric R1 substitution sites, and the TT unit connected with R2 substitution site is shown in blue. Four polymers composed of different alkyl side chain (ethylhexyl group and dodecyl group) substituion combinations are shown in different colors.

For TDTR measurements, a 100 nm-thick (nominal thickness) aluminium film was deposited on top of each BHJ film using electron beam evaporation. The pump-probe setup used for measuring the thermal conductivity has been described previously[18]. The total laser power applied on the sample surface is around 25 mW, which gives an estimated steady state temperature rise of 6-20 K in different BHJs by taking into account the glass substrate as the heat sink[38]. The thermal conductivity is obtained by fitting the phase signal demodulated from the lock-in amplifier using a pulse accumulated model[39] (example TDTR data and fittings are available in SI-figure 1). In the fitting procedure, the specific heat capacities are needed as inputs. Following Duda *et al.*'s approach[30], we use a linear combination of polymer heat capacity and PCBM heat capacity according to their volumetric ratio.

The Atomic Force Microscopy (AFM) measurements were conducted in the tapping mode using a Bioscope II microscope system with a nanoscope V controller (Veeco Inc. USA).

The transmission light microscopy images were obtained by focusing a 660 nm laser beam with a TIRF 60x oil immersion objective (1.49 NA, Nikon Inc.) on the blend film surface and performing a two-dimensional, point-by-point scan with a step size of 50 nm using a high precision piezo stage (P-527.3Cl, PhysikInstrumente). The transmitted light was detected by an avalanche photodiode (Hamamatsu C5331-12).

Results and discussion

The thermal conductivities of pure PBDTTT polymer phase for each of the polymers used in this work have been determined previously[18]. For the PCBM phase, a few research groups have determined its thermal conductivity[19, 20]. Considering that the sample preparation methods and sample purity may influence the thermal conductivity, we performed independent TDTR measurements on neat PCBM films to eliminate the uncertainty these factors may introduce in analyzing the thermal conductivity data. The PCBM films were prepared using the

same spin cast protocol as was used for obtaining the BHJ films and their thicknesses are found to be 50-70 nm. Our measured PCBM thermal conductivity is 0.07±0.007 $Wm^{-1}K^{-1}$ when using a volumetric heat capacity of 1.3×10^{6} $Jm^{-3}K^{-1}$, which was used in Refs [19, 20]. This thermal conductivity we obtained is higher than one reported value of ~0.03 $Wm^{-1}K^{-1}$ [20], but in good agreement with the thermal conductivity reported for a PCBM film prepared using spin casting and without annealing[19] .

In Figure 2, we summarize the thermal conductivity measured for all four types of BHJs with different polymer concentrations. A general and consistent trend in all four polymer BHJs is that as the polymer concentration increases, the thermal conductivity first slightly decreases and then starts to increase when the polymer concentration reaches ~30-35%. This is different from the trend previously observed by Duda et al [30] on P3HT:PCBM blends which show a linear relation. It is possible that the PBDTTT polymers used in this work have different mixing behavior with PCBM compared to P3HT, which further renders different thermal conductivity relationships in the BHJs. PBDTTT is a type of conjugated copolymer, which is usually easier to crystallize than homopolymer like P3HT. Particularly with linear side chain modification, stronger interchain packing takes place in PBDTTT polymers, which tends to prevent efficient PCBM molecule intercalation into the polymer chains and leads to coarse-grained mixing in the BHJs[40-42]. Other factors, such as the difference between P3HT and PBDTTT in molecule orientation preferences in thin films[43,18], may also contribute to the observed different thermal conductivity behaviors. However, more accurate explanation of the difference needs a more detailed atomistic level study, which falls out of the scope of the current study.

In all cases shown in Figure 2, the BHJ thermal conductivity at some concentrations is even lower than pure PCBM by as much as 15% (~0.06 $Wm^{-1}K^{-1}$). Such an observation is surprising since PBDTTT polymers have thermal conductivities larger than that of PCBM. With the presence of polymers in the PCBM, the thermal conductivity of the composite should be larger than the pure PCBM according to conventional composite models, such as EMA.[32] We used the classical Maxwell-Garnett EMA theory[32] to model the thermal conductivity of the BHJs as a function of the compositing ratio.

EMA theory for describing the composite's effective thermal conductivity as a function of inclusion particle concentration is expressed as:

$$\frac{k(\varphi)}{k_h} = \frac{k_p + 2k_h + 2\varphi(k_p - k_h)}{k_p + 2k_h - \varphi(k_p - k_h)} \quad (1)$$

This expression allows us to evaluate the effective thermal conductivity by simply using the thermal conductivities of two compositing phases (k_p and k_h) and the inclusion phase volumetric concentration, φ. Since the major phase changes when the compositing ratios change in the BHJ composites. We performed two sets of calculation using either the polymer or the PCBM as the host phase in Eq. 1 (red and blue solid lines in

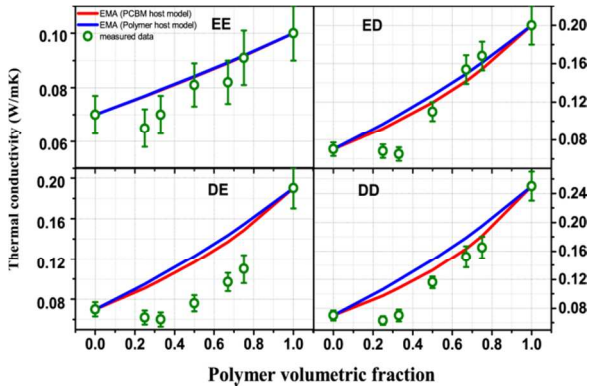

Figure 2. Thermal conductivity changes in four BHJs as a function of polymer volume fraction (green open circle). Blue and red lines are predicted values from EMA model using polymer and PCBM as the host phase, respectively.

Figure 2). This, however, does not make a large difference in the modeling results because of the low contrast ratio of the two constituents' thermal conductivities, and both lines exhibit significant deviation from the experiment data, particularly in the regime of 0-50% polymer volumetric concentration.

One important difference between the BHJs and conventional polymer-inorganic particle composite is that both constituents in the polymer-PCBM composite can break down to molecules when mixing. This brings in a difficulty of describing the thermal conductivity of both phases. As we know, the thermal conductivities used in the EMA are the bulk thermal conductivities of the constituents. However, polymer and PCBM can mix with each other on the molecular level, i.e., molecules or small clusters of one constituent can intercalate into the content-rich domain of the other constituent[44]. The thermal conductivity of the individual molecules can be much larger than that of the bulk amorphous polymer in which thermal transport is dominated by inefficient thermal transport from one molecule to another through a diffusion-like process[45]. Thermal transport within π-conjugated molecule chains is dominated by highly delocalized vibration modes which is very efficient because their chain backbones are very stiff and strong[46]. Even for molecule clusters, depending on their orderings (crystalline or disordered), their thermal conductivity can also be much larger than the amorphous bulk counterpart. As a result, the use of bulk thermal conductivities in the EMA model is problematic. With these factors in mind, it is easier to understand the unusual mixing behavior in the BHJs, although the present experimental and characterization data limit our understanding of the thermal transport mechanism to a qualitatively stage.

Starting from pure PCBM, when polymers are blended in it, the polymers are minor phases. As mentioned above, these polymer

molecules or clusters should have thermal conductivity larger than or equal to their bulk counterpart. According to EMA, the thermal conductivity of the BHJs should be always larger than PCBM. However, we see that the thermal conductivity reduces slightly when polymers are minor phases (Figure 2). There are three possible reasons that can lead to a thermal conductivity decrease of the blend. The first one is that the polymer molecules or clusters work as defects that scatter the heat carriers in the PCBM major phase. This is similar to the alloy effect: when one constituent element has a very low concentration in an alloy, its atoms scatter the phonon transport in the major phase and thus reduce the thermal conductivity. Such a possibility, however, is low since PCBM is disordered and has ultra-low thermal conductivity. The phonon-like propagating heat carriers are not expected to have large contribution to the thermal conductivity, and thus the scattering effect of the polymer molecule/clusters should not be important. The second possibility is that the polymer molecules intercalated into the PCBM phase present lots of interfaces between the PCBM and the polymer molecules. The thermal transport between PCBM and polymer molecules is dominated by weak van der Waals interactions and the thermal conductance of such interfaces are usually on the order of 10 $MWm^{-2}K^{-1}$. Considering that the thermal conductivity of PCBM is 0.07 $Wm^{-1}K^{-1}$, this interfacial resistance is equivalent to a 7 nm-thick PCBM layer which is on the same order as the size of the PCBM microstructures (shown later in GIXS data, Table 1). As more such interfaces are created by more polymer molecules, the thermal conductivity of the composite will be lowered. The third possibility is related to the special feature of PCBM. Duda et al.[20] hypothesized that the low thermal conductivity of PCBM is related to the vibrational state of the molecular tail attached to the PCBM molecules which lower the sound speed as well as the characteristic frequencies. Although such an argument has not been proven, if it is true, it can be a reason of the lower thermal conductivity of the blend. The vibration of the polymer intercalated into the PCBM phase may have the same effect as that from the molecular tail attached to PCBM, which in turn lower the thermal conductivity.

After 35% polymer concentration, the thermal conductivities of all four BHJs start to ramp up. Possible explanation for this is that when the polymer content is beyond some threshold concentration, certain percolation phenomenon might have taken place in the composite. Such percolation forms a long range network of polymer which allows a low thermal resistance pathway, and the composite's effective thermal conductivity shall increase more significantly after passing the percolation threshold. Another observation is that BHJs with EE and ED polymers seem to have larger curvatures around the 30-35% polymer ratio than the DE and DD cases. We believe that this reflects different percolation behavior of the different polymers in the BHJs and is related to the phase segregation as well as the molecular packing. Our previous study indicates that from EE to DD, the ability to form crystal becomes larger[18]. Here, we performed AFM measurements to characterize surface morphology associated with phase segregation (Figure. 3a). The BHJs loaded with 50% EE obviously form more finely mixed phases, while BHJs loaded with DD, which tends to aggregate more easily, form much coarser phases.

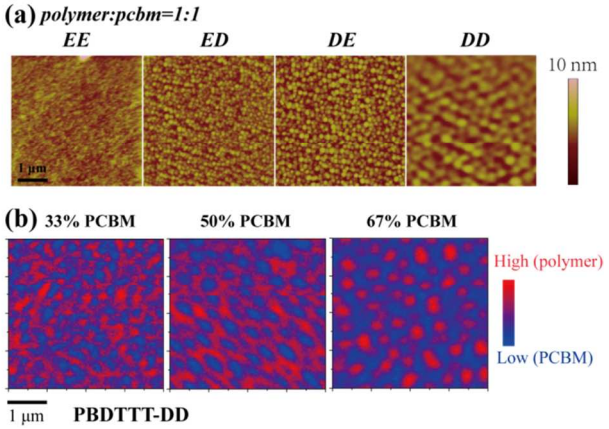

Figure 3. (a) AFM height images of BHJ film morphologies. Four different polymer BHJs with 50% PCBM loading are shown. (b) Transmission microscopy imaging of PBDTTT-DD:PCBM BHJs at different mixing ratios. Red color represents polymer rich regions, and blue color represents PCBM rich regions.

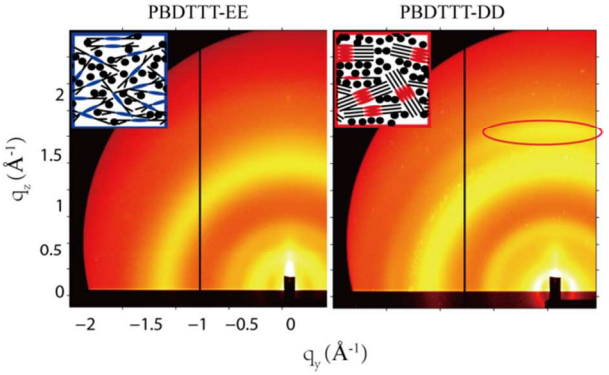

Figure 4. GIWAXS data for BHJ thin films with 50% PCBM loading. Scattering due to π-π stacking is present in PBDTTT-DD BHJ films (right, regions inside the red oval), but absent in PBDTTT-EE BHJ films (left). The π-π stacking shows a preferred orientation along the out-of-plane direction. In each case, the more homogenous scattering ring at shorter wave vector is due to PCBM. Insets: Schematic diagram showing the PCBM molecular packing with two different polymer chains.

We further characterized and assigned the composition of each domain observed in the AFM images by the transmission microscopy experiment. The transmission microscopy imaging of PBDTTT-DD BHJs at different PCBM concentrations is shown in Figure 3b. Since the probing wavelength (660 nm) was set at the absorption peak of PBDTTT polymer, yet PCBM molecules have very low absorption cross section at this wavelength, the high absorption regions found in the images correspond to the polymer-rich domains while low absorption

regions denote the PCBM-rich domains. One important observation from these images is that at lower polymer volumetric fraction, for example, in 67% PCBM BHJs, the polymer rich regions are still isolated by the PCBM, and no obvious high thermal conductivity pathway can be formed.

Table 1. Polymer/PCBM nano-crystallite size in PBDTTT-EE/PBDTTT-DD BHJs obtained by first fitting the full width half maxima of π-π stacking scattering peak with gaussian functions and then converting them using Scherrer's equation[48]. The broad peak widths did not require correction for the instrumental resolution[49], which could resolve coherence lengths about an order of magnitude larger than those observed[47].

PCBM (%)	Polymer nano-crystallite size (nm) (EE/DD)	PCBM aggregate size (nm) (EE/DD)
25	1.2¶/5.9	N.A./1.2
50	N.A./4.0	2.0/2.2
75	N.A./4.2	2.1/2.0

¶This crystallite size represents PCBM-intercalated polymer nano-crystalites (see supporting information)

*N.A., not available

However, when the polymer concentration is increased to 50%, long range network of polymer-rich region has been formed and become even more densely interconnected at even higher polymer volumetric fraction. This further supports previous speculation about forming high thermal conductivity pathway through the polymer-rich domains.

To further characterize the microstructures of BHJs, we performed grazing incidence wide angle x-ray scattering (GIWAXS) experiments at Beamline 8-ID-E of the Advanced Photon Source[47]. From the data, we extracted the local structural order and characteristic dimensions (Figure 4 and Table 1). We found that for the BHJs with the DD polymer, small polymer crystallites always exist, even with a polymer volumetric fraction as low as 25% (Table 1). On the other hand, for BHJs with EE polymers, introducing PCBM causes the π-π stacking scattering features to undergo a shift to longer characteristic length instead of simply lowering its intensity (see supporting information SI-figure 2), and eventually eliminates the π-π stacking scattering features. These facts point to a picture that PCBM molecules are well intercalated into the EE polymer structure but not in that of the DD polymer (Figure 4)[22]. This conclusion is in good agreement with previous finding from GISAXS measurements of this type of BHJs[31]. As a result, with the same concentration of polymers, the EE polymer, compared to DD, will tend to spread to a larger volume and be more likely to form a percolated network (see schematics in Figure 4). This could be the reason why we see faster increases in the thermal conductivities of EE and ED than in the DE and DD cases around the polymer concentration of 30-35%.

Conclusions

The thermal conductivity of PBDTTT:PCBM BHJ films as a function of polymer volume fraction has been measured by TDTR. The data cannot be adequately described by conventional effective medium theory using either polymer or PCBM as the host phase. Surprisingly, when the polymer volumetric fraction is below 35%, all four types of polymer BHJs have slightly lower thermal conductivities than the pure PCBM phase. Formation of a high-thermal-conductivity interconnected polymer network by percolation may explain the thermal conductivity increase observed for polymer concentration exceeding 30-35%. Different percolation behavior between polymer BHJs might be related to their phase segregation behavior and host molecular intercalation details. The results suggest that molecular level mixing of the binary phases is important in considering the heat transfer problem of BHJ polymer solar cells.

Acknowledgements

This work is funded by the Sustainable Energy Initiative (SEI) at the University of Notre Dame. This research used resources of the Advanced Photon Source, a U.S. Department of Energy (DOE) Office of Science User Facility operated for the DOE Office of Science by Argonne National Laboratory under Contract No. DE-AC02-06CH11357.

Notes and references

[a] Department of Aerospace and Mechanical Engineering, University of Notre Dame, Notre Dame, Indiana, 46556, USA.
[b] Department of Chemistry and Biochemistry, University of Notre Dame, Notre Dame, Indiana, 46556, USA.
[c] X-Ray Science Division, Argonne National Laboratory, Argonne, IL 60439, USA.
[d] Department of Chemistry, Purdue University, West Lafayette, IN 47907, USA
[e] Department of Physics, Illinois Institute of Technology, Chicago, IL 60616 and Center for Synchrotron Radiation Research and Instrumentation (CSRRI) Argonne National Laboratory, Argonne, IL 60439, USA
[f] Center for Sustainable Energy of Notre Dame, University of Notre Dame, Notre Dame, IN 46556, USA

.

Electronic Supplementary Information (ESI) available: Example TDTR data and GIWAXS pattern line cuts of PBDTTT-EE and PBDTTT-DD BHJs with different PCBM volumetric fractions are included in the supplemental information. See DOI: 10.1039/b000000x/

1. J. You, L. Dou, K. Yoshimura, T. Kato, K. Ohya, T. Moriarty, K. Emery, C.-C. Chen, J. Gao and G. Li, *Nature communications*, 2013, 4, 1446.
2. F. C. Krebs, *Solar Energy Materials and Solar Cells*, 2009, 93, 394-412.

3. H.-Y. Chen, J. Hou, S. Zhang, Y. Liang, G. Yang, Y. Yang, L. Yu, Y. Wu and G. Li, *Nat Photon*, 2009, 3, 649-653.
4. S. Bertho, I. Haeldermans, A. Swinnen, W. Moons, T. Martens, L. Lutsen, D. Vanderzande, J. Manca, A. Senes and A. Bonfiglio, *Solar Energy Materials and Solar Cells*, 2007, 91, 385-389.
5. X. Yang, J. K. J. van Duren, R. A. J. Janssen, M. A. J. Michels and J. Loos, *Macromolecules*, 2004, 37, 2151-2158.
6. F. Padinger, T. Fromherz, P. Denk, C. Brabec, J. Zettner, T. Hierl and N. Sariciftci, *Synthetic metals*, 2001, 121, 1605-1606.
7. M. Jørgensen, K. Norrman and F. C. Krebs, *Solar Energy Materials and Solar Cells*, 2008, 92, 686-714.
8. J. M. Kroon, M. M. Wienk, W. J. H. Verhees and J. C. Hummelen, *Thin Solid Films*, 2002, 403–404, 223-228.
9. L. H. Sperling, *Introduction to physical polymer science*, John Wiley & Sons, 2005.
10. T. Luo and G. Chen, *Physical Chemistry Chemical Physics*, 2013, 15, 3389-3412.
11. T. Zhang and T. Luo, *ACS nano*, 2013, 7, 7592-7600.
12. T. Zhang and T. Luo, *Journal of Applied Physics*, 2012, 112, 094304.
13. Z. Zhong, M. C. Wingert, J. Strzalka, H.-H. Wang, T. Sun, J. Wang, R. Chen and Z. Jiang, *Nanoscale*, 2014, 6, 8283-8291.
14. S. Shen, A. Henry, J. Tong, R. Zheng and G. Chen, *Nat Nano*, 2010, 5, 251-255.
15. A. Henry, G. Chen, S. J. Plimpton and A. Thompson, *Physical Review B*, 2010, 82, 144308.
16. T. Luo, K. Esfarjani, J. Shiomi, A. Henry and G. Chen, *Journal of Applied Physics*, 2011, 109, -.
17. V. Singh, T. L. Bougher, A. Weathers, Y. Cai, K. Bi, M. T. Pettes, S. A. McMenamin, W. Lv, D. P. Resler, T. R. Gattuso, D. H. Altman, K. H. Sandhage, L. Shi, A. Henry and B. A. Cola, *Nat Nano*, 2014, 9, 384-390.
18. Z. Guo, D. Lee, Y. Liu, F. Sun, A. Sliwinski, H. Gao, P. C. Burns, L. Huang and T. Luo, *Physical Chemistry Chemical Physics*, 2014, 16, 7764-7771.
19. X. Wang, V. Ho, R. A. Segalman and D. G. Cahill, *Macromolecules*, 2013, 46, 4937-4943.
20. J. C. Duda, P. E. Hopkins, Y. Shen and M. C. Gupta, *Physical review letters*, 2013, 110, 015902.
21. X. Guo, M. Zhang, J. Tan, S. Zhang, L. Huo, W. Hu, Y. Li and J. Hou, *Advanced Materials*, 2012, 24, 6536-6541.
22. A. Mayer, M. F. Toney, S. R. Scully, J. Rivnay, C. J. Brabec, M. Scharber, M. Koppe, M. Heeney, I. McCulloch and M. D. McGehee, *Advanced Functional Materials*, 2009, 19, 1173-1179.
23. T. Luo and J. R. Lloyd, *Advanced Functional Materials*, 2012, 22, 2495-2502.
24. E.-S. Lee, S.-M. Lee, D. J. Shanefield and W. R. Cannon, *Journal of the American Ceramic Society*, 2008, 91, 1169-1174.
25. R. F. Hill and P. H. Supancic, *Journal of the American Ceramic Society*, 2002, 85, 851-857.
26. Y. P. Mamunya, V. Davydenko, P. Pissis and E. Lebedev, *European polymer journal*, 2002, 38, 1887-1897.
27. G.-W. Lee, M. Park, J. Kim, J. I. Lee and H. G. Yoon, *Composites Part A: Applied Science and Manufacturing*, 2006, 37, 727-734.
28. Z. Han and A. Fina, *Progress in polymer science*, 2011, 36, 914-944.
29. B. Weidenfeller, M. Höfer and F. R. Schilling, *Composites Part A: Applied Science and Manufacturing*, 2004, 35, 423-429.
30. J. C. Duda, P. E. Hopkins, Y. Shen and M. C. Gupta, *Applied Physics Letters*, 2013, 102, 251912.
31. Z. Guo, D. Lee, R. D. Schaller, X. Zuo, B. Lee, T. Luo, H. Gao and L. Huang, *Journal of the American Chemical Society*, 2014, 136, 10024-10032.
32. J. M. Garnett, *Philosophical Transactions of the Royal Society of London. Series A, Containing Papers of a Mathematical or Physical Character*, 1904, 385-420.
33. E. F. Jordan, D. W. Feldeisen and A. N. Wrigley, *Journal of Polymer Science Part A-1: Polymer Chemistry*, 1971, 9, 1835-1851.
34. C. Cabanetos, A. El Labban, J. A. Bartelt, J. D. Douglas, W. R. Mateker, J. M. J. Fréchet, M. D. McGehee and P. M. Beaujuge, *Journal of the American Chemical Society*, 2013, 135, 4656-4659.
35. J. Guo, Y. Liang, J. Szarko, B. Lee, H. J. Son, B. S. Rolczynski, L. Yu and L. X. Chen, *The Journal of Physical Chemistry B*, 2009, 114, 742-748.
36. D. Mühlbacher, M. Scharber, M. Morana, Z. Zhu, D. Waller, R. Gaudiana and C. Brabec, *Advanced Materials*, 2006, 18, 2884-2889.
37. C. Soci, I. W. Hwang, D. Moses, Z. Zhu, D. Waller, R. Gaudiana, C. J. Brabec and A. J. Heeger, *Advanced Functional Materials*, 2007, 17, 632-636.
38. D. G. Cahill, *Review of Scientific Instruments*, 2004, 75, 5119-5122.
39. A. J. Schmidt, Massachusetts Institute of Technology, 2008.
40. J. A. Bartelt, J. D. Douglas, W. R. Mateker, A. E. Labban, C. J. Tassone, M. F. Toney, J. M. J. Fréchet, P. M. Beaujuge and M. D. McGehee, *Advanced Energy Materials*, 2014, 4, n/a-n/a.
41. J. S. Moon, C. J. Takacs, S. Cho, R. C. Coffin, H. Kim, G. C. Bazan and A. J. Heeger, *Nano letters*, 2010, 10, 4005-4008.
42. Y. Liang, Z. Xu, J. Xia, S. T. Tsai, Y. Wu, G. Li, C. Ray and L. Yu, *Advanced Materials*, 2010, 22, E135-E138.
43. H. Yang, S. W. LeFevre, C. Y. Ryu and Z. Bao, *Applied Physics Letters*, 2007, 90, 172116-172116-172113.
44. W. Chen, T. Xu, F. He, W. Wang, C. Wang, J. Strzalka, Y. Liu, J. Wen, D. J. Miller and J. Chen, *Nano letters*, 2011, 11, 3707-3713.
45. P. B. Allen and J. L. Feldman, *Physical Review B*, 1993, 48, 12581.
46. T. Zhang, X. Wu and T. Luo, *The Journal of Physical Chemistry C*, 2014, DOI: 10.1021/jp5051639.
47. Z. Jiang, X. Li, J. Strzalka, M. Sprung, T. Sun, A. R. Sandy, S. Narayanan, D. R. Lee and J. Wang, *Journal of Synchrotron Radiation*, 2012, 19, 627-636.
48. S. Stock and B. Cullity, *Prentice Hall, Upper Saddle River, NJ*, 2001.
49. D.-M. Smilgies, *Journal of Applied Crystallography*, 2009, 42, 1030-1034.

